

PLANETS NEAR MEAN-MOTION RESONANCES

CRISTOBAL PETROVICH¹, RENU MALHOTRA², & SCOTT TREMAINE³

Draft version March 6, 2022

ABSTRACT

The multiple-planet systems discovered by the *Kepler* mission exhibit the following feature: planet pairs near first-order mean-motion resonances prefer orbits just outside the nominal resonance, while avoiding those just inside the resonance. We explore an extremely simple dynamical model for planet formation, in which planets grow in mass at a prescribed rate without orbital migration or dissipation. We develop an analytic version of this model for two-planet systems in two limiting cases: the planet mass grows quickly or slowly relative to the characteristic resonant libration time. In both cases the distribution of systems in period ratio develops a characteristic asymmetric peak-trough structure around the resonance, qualitatively similar to that observed in the *Kepler* sample. We verify this result with numerical integrations of the restricted three-body problem. We show that for the 3:2 resonance, where the observed peak-trough structure is strongest, our simple model is consistent with the observations for a range of mean planet masses 20–100 M_{\oplus} . This mass range is higher than expected, by at least a factor of three, from the few *Kepler* planets with measured masses, but part of this discrepancy could be due to oversimplifications in the dynamical model or uncertainties in the planetary mass-radius relation.

Subject headings: planetary systems – planets and satellites: dynamical evolution and stability – planets and satellites: formation

1. INTRODUCTION

As of fall 2012, almost 100 multi-planet systems have been detected by ground-based radial-velocity observations, and 365 transiting multi-planet systems have been detected by the *Kepler* spacecraft⁴. These large samples enable statistical studies of correlations between the properties of members of multi-planet systems. One result from these studies is that many planets appear to be close to mean-motion resonances, that is, their orbital periods are close to the ratio of two small integers (see below for a more precise definition). In particular:

- Lissauer et al. (2011b) comment that about one-third of the multi-planet systems studied by radial-velocity measurements contain near-resonant planet pairs, with about half of these near the 2:1 resonance. This is probably an underestimate because of a detection bias: there is an approximate degeneracy between the signal from an interior planet near the 2:1 resonance and harmonics arising from non-zero eccentricity in the outer planet orbit, which makes it difficult to detect low-mass planets in resonance with exterior companions (e.g., Anglada-Escudé et al. 2010).
- Fabrycky et al. (2012) find that *Kepler* planet pairs with orbital period ratios within a few percent of 2:1 or 3:2 are preferentially found just wide of the

resonance (i.e., period ratio slightly larger than 2 or 1.5) and tend to avoid spacings just narrow of the resonance.

- Near-resonances involving three or more planets are also present in the *Kepler* data. Lissauer et al. (2011b) find that the four planets in the system KOI-730 are in a chain of resonances, with period ratios 8:6:4:3 to within 0.1%. Lissauer et al. also find strong evidence for other resonances, including two three-planet resonances in the five-planet system KOI-500. Fabrycky et al. (2012) find that three planets in the systems KOI-720 and KOI-2086 have mean motions n that satisfy $5n_2 - 3n_4 - 2n_1 \simeq 0$ and $n_1 - 2n_2 + n_3 \simeq 0$ respectively, to within 0.01% (the planets are labeled in order of increasing period).
- In the GJ 876 system, planets 2, 3, and 4 have periods close to the ratio 1:2:4; planets 2 and 3 are close to a secular resonance; and there are other probable near-resonances (see Baluev 2011 and references therein). Because of these near-resonances, gravitational interactions between the planets are detectable in the radial-velocity data, and these can be used to constrain the mutual inclinations and determine whether various critical arguments librate or circulate.
- Within the solar system, Jupiter and Saturn are within 1% of a 5:2 resonance (the “great inequality”), Uranus and Neptune are within 2% of a 2:1 resonance, and Pluto is in a 3:2 resonance with Neptune. There are also many resonances among the satellites of Jupiter and Saturn. Another notable near-resonance occurs between the two outer planets of the pulsar PSR B1257+12, which are

¹ Department of Astrophysical Sciences, Princeton University, Ivy Lane, Princeton, NJ 08544, USA; cpetrovi@princeton.edu

² Lunar and Planetary Laboratory, The University of Arizona, Tucson, AZ 85721, USA; renu@lpl.arizona.edu

³ School of Natural Sciences, Institute for Advanced Study, Einstein Drive, Princeton, NJ 08540, USA; tremaine@ias.edu

⁴ Technically most of these are planet candidates, since they have not been confirmed by radial-velocity measurements, but the expected false-positive rate in multi-planet transiting systems is quite low (Lissauer et al. 2012).

within 2% of a 3:2 resonance. This near-resonance produces gravitational interactions large enough to be easily detectable, which allowed the existence of the planets to be confirmed and their inclinations to be measured shortly after their discovery (Rasio et al. 1992; Malhotra et al. 1992).

Loosely speaking, an orbital resonance between two planets occurs when their mean motions or orbital frequencies n_1, n_2 are nearly commensurate, i.e., n_1/n_2 is close to a ratio of small integers, $p : p+q$ where $p \neq 0$ and $q \geq 0$. The case $q = 0$ is sometimes called a corotation or co-orbital resonance; examples in the solar system include the Trojan asteroids (1:1 resonance with Jupiter) and the Saturnian satellites Janus and Epimetheus, but no extrasolar co-orbital resonances are known. When $q > 0$ it is called the order of the resonance, since for planets on nearly circular, coplanar orbits the strength of the resonance potential is proportional to e^q or I^q where e and I are the eccentricities and inclinations of the resonant planets. Inclination resonances occur only for even q .

In a resonant configuration, the longitude of the planets at every q th conjunction librates slowly about a direction determined by the lines of apsides and nodes of the planetary orbits. In the action-angle variables for the Keplerian potential, this geometry is naturally described by the libration of a so-called critical argument which is a linear combination of the angle variables (Malhotra 1994, 1998; Murray & Dermott 1999).

Definition of resonance— Generally, a planet pair is said to be “in resonance” if some dynamically significant critical argument librates. If the critical argument circulates the planet pair is said to be near but not in resonance. This definition has several shortcomings for our purposes (see for example Henrard & Lemaître 1983; Delisle et al. 2012): (i) it is not always consistent with the expectation that resonant planets have orbital periods close to the ratio of two small integers, since planets can be resonant at *any* period ratio⁵; (ii) by suitable canonical transformations one can change the appropriate critical argument from libration to circulation, so this definition of resonance is coordinate-dependent; (iii) interaction of nearby resonances arising from the degenerate frequencies in the Kepler problem can cause a critical argument to jump between libration and circulation at irregular intervals.

Given these comments, it is nugatory to discuss whether *Kepler*’s multi-planet systems are “resonant” or “non-resonant”, and in this paper we shall avoid the term “resonant” in favor of the looser description “near-resonant”.

Resonances and migration— Convergent migration—evolution of the semi-major axis of one or both planets such that the period ratio approaches unity—can lead to permanent capture into resonance, and is believed to be the cause of the Neptune-Pluto resonance (Malhotra 1993) and the resonances between satellites of Jupiter

and Saturn (although in these cases the migration is outward, whereas migration in most exoplanet systems is believed to be inward).

The existence of near-resonant planet pairs is often ascribed to convergent migration (e.g., Snellgrove et al. 2001), but there are problems with this hypothesis:

- The fraction of planets in resonance is quite small: Fabrycky et al. (2012) find peaks at the 3:2 and 2:1 resonances of ~ 20 planet pairs each, out of a total sample of ~ 750 planet pairs; this small fraction is noteworthy since capture into the 2:1 resonance is certain during convergent migration if the planets cross the resonance slowly enough and their initial eccentricities and inclinations are small enough. “Slowly enough” means a migration timescale larger than $10^4 \text{ yr} (P_{\text{pl}}/100 \text{ d})(10M_{\oplus}/m_{\text{pl}})^{4/3}$ where m_{pl} and P_{pl} are the migrating planet’s mass and orbital period; “small enough” means initial eccentricity smaller than $0.05(m_{\text{pl}}/10M_{\oplus})^{1/3}$ (see Appendix). Typical Type I migration times for *Kepler* planets in a low-mass protoplanetary disk are 10^3 – 10^4 yr (Tanaka et al. 2002), in which case migrating planets might avoid resonance capture according to this criterion, but orbit integrations by Rein (2012) that include eccentricity damping show that most *Kepler* planets are captured even if the migration time is as short as 10^3 yr.
- Convergent migration typically leads to capture into a 2:1 resonance. Capture into resonances with smaller separations, such as 3:2 or 4:3, becomes increasingly difficult: for example, to capture a planet into the 3:2 resonance requires either that the initial conditions are fine-tuned so that the planets form in the narrow interval between the 2:1 and 3:2 resonance (only 13% of the outer planet’s semi-major axis), or that the migration rate is fast enough that the planet jumps the weaker 2:1 and is captured at the 3:2 resonance. Yet Fabrycky et al. (2012) find that the excess of planet pairs near the 3:2 resonance is at least as strong as the excess at the 2:1 resonance (see Rein et al. 2012 for a detailed numerical study of these issues).
- In the sample of *Kepler* multi-planet systems examined by Fabrycky et al. (2012), the excess of planet pairs at period ratios just larger than 2 is accompanied by a deficit at period ratios just smaller than 2. Both the peak and the trough have an equivalent width of about 20 planets. This strongly suggests that the features at this resonance arise from rearranging the periods of planets near the resonance, rather than by capturing planets at the resonance, which should produce a peak but no trough.

Batygin & Morbidelli (2012) and Lithwick & Wu (2012) have pointed out that dissipation due to tides from the host star or the protoplanetary disk tends to repel near-resonant planets, in the sense that their period ratios evolve away from unity (see also Delisle et al. 2012). Thus, if migration is common, dissipation could explain why there are so few near-resonant planet pairs;

⁵ As the eccentricity approaches zero, the apsidal precession rate due to a perturber grows without limit. Thus a critical angle whose time derivative involves the mean motions and precession rate can librate even when the mean motions are far from commensurability.

and if there is little or no migration, dissipation could explain why planet pairs that initially happen to lie near a resonance are now preferentially found wide of the resonance. This hypothesis is discussed further in §7.3.

Although these and other analyses in the literature shed considerable light on the behavior of near-resonant planets in the presence of dissipation and/or migration, our view is that they put the cart before the horse: the question that should be addressed first is, what is the distribution of mean motions or period ratios expected near a resonance in the *absence* of dissipation or migration?

Efforts to address this question have a long and rich history, mostly in the context of the asteroid belt, in which the distribution of mean motions contains gaps at the 4:1, 3:1, 5:2, 7:3, and 2:1 resonances with Jupiter (the Kirkwood gaps) and peaks at the 3:2 and 1:1 resonances (the Hilda family and the Trojan asteroids). Most of these features can be largely explained through chaotic evolution of the asteroid orbits on timescales as long as 1 Gyr, long after the formation of the solar system was complete (Wisdom 1983; Murray & Holman 1997; Lecar et al. 2001). Although the effects of dissipation and migration are discernible in the orbital distribution of asteroids, these features are comparatively subtle (Liou & Malhotra 1997; Minton & Malhotra 2009, 2010). Thus the asteroid belt demonstrates that dissipation and large-scale migration are not essential to produce near-resonant features in the mean-motion distribution. Unfortunately for our purposes, the chaotic evolution of the asteroids appears to depend strongly on the details of the planetary configuration in the solar system and thus the insights gained from studies of the asteroid belt cannot be immediately applied to exoplanets.

In this paper we focus on a simple and highly idealized model for the formation of near-resonant features: at an initial time $t = 0$ we place a single planet and a large number of test particles on circular orbits around the host star. The test particles are interior to the planet and smoothly distributed in semi-major axis (see Equation 41). The mass of the planet is $m_{\text{pl}}h(t)$ where $h(t)$ ramps up from zero at time zero to unity at large times; we focus on the two limiting cases in which the planet mass grows rapidly— $h(t)$ is a step function at $t = 0$ —and slowly compared to the characteristic orbital and secular frequencies of the test particles; see Equation (38).

2. ANALYTIC RESULTS

2.1. Orbital elements

We follow the motion of the test particles using osculating Keplerian orbital elements, with a, e, ω, ℓ being the semi-major axis, eccentricity, longitude of periapsis and mean anomaly. For canonical elements we use the modified Delaunay variables $\lambda = \ell + \omega, \gamma = -\omega, \Lambda = (\mu a)^{1/2}, \Gamma = (\mu a)^{1/2}[1 - (1 - e^2)^{1/2}]$, where $\mu = Gm_*$ is the gravitational mass of the star.

The Hamiltonian for the restricted three-body problem (star, planet, test particle) is

$$\begin{aligned} H(\lambda, \gamma, \Lambda, \Gamma, t) &= -\frac{\mu^2}{2\Lambda^2} - \mu_{\text{pl}} \left[\frac{1}{|\mathbf{r} - \mathbf{r}_{\text{pl}}|} - \frac{\mathbf{r} \cdot \mathbf{r}_{\text{pl}}}{r_{\text{pl}}^3} \right] \\ &= -\frac{\mu^2}{2\Lambda^2} + \mu_{\text{pl}} H_{\text{pl}}(\lambda, \gamma, \Lambda, \Gamma, t) \end{aligned} \quad (1)$$

where $\mu_{\text{pl}} = Gm_{\text{pl}}$ is the gravitational mass of the planet and $\mathbf{r}, \mathbf{r}_{\text{pl}}$ are the position vectors of the test particle and planet relative to the star. The first term describes the unperturbed Keplerian motion of the test particle about the Sun, and the remainder describes the perturbation from the planet.

Transit observations of exoplanets measure the time interval P_{tr} between successive transits, that is, the interval in which the longitude increases by 2π . We must relate the transit-based mean motion $n_{\text{tr}} \equiv 2\pi/P_{\text{tr}}$ to the osculating mean motion n , given by $n^2 = \mu/a^3$. Write the perturbing Hamiltonian as

$$H_{\text{pl}}(\lambda, \gamma, \Lambda, \Gamma, t) = H_{\text{lp}}(\gamma, \Lambda, \Gamma, t) + H_{\text{sp}}(\lambda, \gamma, \Lambda, \Gamma, t) \quad (2)$$

where

$$H_{\text{lp}} = \langle H_{\text{pl}} \rangle_t, \quad H_{\text{sp}} = H_{\text{pl}} - H_{\text{lp}}, \quad (3)$$

with $\langle \cdot \rangle_t$ denoting a time average over an interval comparable to the total observational timespan; H_{sp} and H_{lp} are respectively the short-period and long-period parts of the Hamiltonian. Then n_{tr} is the time average of the rate of change of the mean longitude, $n_{\text{tr}} = \langle d\lambda/dt \rangle_t$, and we have

$$n_{\text{tr}} = \left\langle \frac{d\lambda}{dt} \right\rangle_t = \left\langle \frac{\partial H}{\partial \Lambda} \right\rangle_t = \frac{\mu^2}{\Lambda^3} + \frac{\partial H_{\text{lp}}}{\partial \Lambda} = n + \frac{\partial H_{\text{lp}}}{\partial \Lambda} \quad (4)$$

where n is the osculating mean motion.

For the resonances we shall examine, the second term in these equations is small; thus we may neglect the distinction between n and n_{tr} . In other words, the distribution of transit-based period ratios near resonances is determined mainly by the distribution of the osculating mean motions rather than by any differences between the osculating and transit-based mean motions.

2.2. Resonant dynamics

We consider the vicinity of a first-order mean-motion resonance, where the ratio of the mean motions of the planet and the test particle is $p : (p+1)$. Thus $p > 0$ corresponds to an interior resonance (test particle inside the planet) and $p < -1$ is an exterior resonance.

We now assume that the resonances are sufficiently well separated compared to the size of the perturbations induced by the planet that we can ignore all of the perturbations except those associated with the $p : (p+1)$ resonance (we call this the single-resonance approximation). It is useful to make a canonical transformation to slow and fast variables,

$$\begin{aligned} \phi &= (p+1)\lambda_{\text{pl}} - p\lambda + \gamma, & \Phi &= \Gamma; \\ \psi &= \lambda - \lambda_{\text{pl}}, & \Psi &= \Lambda + p\Gamma, \end{aligned} \quad (5)$$

where $\lambda_{\text{pl}} = n_{\text{pl}}(t - t_0)$ is the mean longitude of the planet, and n_{pl} is its mean motion. Then the new Hamiltonian is

$$\begin{aligned} \tilde{H} &= n_{\text{pl}}[(p+1)\Phi - \Psi] - \frac{\mu^2}{2(\Psi - p\Phi)^2} \\ &\quad + \mu_{\text{pl}} H_{\text{pl}}(\phi, \psi, \Phi, \Psi; a_{\text{pl}}, e_{\text{pl}}) \end{aligned} \quad (6)$$

where a_{pl} is the semi-major axis of the planet's orbit and H_{pl} represents the planetary perturbation. For simplicity we have assumed that the planet is on a circular orbit and that the test-particle and planet orbits are coplanar. Since ψ is a fast variable, we will drop ψ -dependent

terms, which is equivalent to replacing H_{pl} by H_{lp} ; consequently, the resonance Hamiltonian is independent of ψ and Ψ is a constant of the motion. We shall use the notation

$$n_c = \frac{\mu^2}{\Psi^3}, \quad a_c = \frac{\Psi^2}{\mu}; \quad (7)$$

n_c and a_c are constants of the motion which equal the osculating mean motion and semi-major axis of the test particle when its eccentricity is zero.

If the test-particle orbit is nearly circular, $\Phi \simeq \frac{1}{2}\sqrt{\mu a}e^2$ is small, and we can approximate Equation (6) with a few terms in an expansion in powers of $\sqrt{\Phi}$,

$$\tilde{H}_{\text{res}} = [(p+1)n_{\text{pl}} - pn_c]\Phi + \beta\Phi^2 + \varepsilon\sqrt{2\Phi}\cos\phi, \quad (8)$$

where we have dropped an inessential constant, and

$$\beta = -\frac{3p^2n_c}{2\Psi}, \quad \varepsilon = -\frac{\mu_{\text{pl}}}{a_{\text{pl}}}\frac{f_p}{\sqrt{\Psi}}. \quad (9)$$

Note that $\Psi \simeq \sqrt{\mu a}(1 + \frac{1}{2}pe^2)$, and since the eccentricity is small, we have $\Psi > 0$ and $\beta < 0$ in all cases of interest. The coefficient f_p is given by (Murray & Dermott 1999)

$$f_p = -(p+1 + \frac{1}{2}D)b_{1/2}^{(p+1)}(\alpha), \quad \alpha = [p/(p+1)]^{2/3} \quad (10)$$

when $p > 0$ (planet exterior to test particle), and

$$f_p = -\alpha(p + \frac{1}{2} - \frac{1}{2}D)b_{1/2}^{(p+1)}(\alpha) - \frac{\delta_{p,-2}}{2\alpha}, \quad \alpha = [(p+1)/p]^{2/3} \quad (11)$$

when $p < -1$ (planet interior to test particle). Here $\delta_{i,j}$ is the Kronecker delta function, $D \equiv d/d\log\alpha$, and the Laplace coefficient

$$b_{1/2}^{(m)}(\alpha) = \frac{1}{\pi} \int_0^{2\pi} \frac{\cos mx \, dx}{(1 - 2\alpha \cos x + \alpha^2)^{1/2}}. \quad (12)$$

We have

$$\begin{aligned} f_1 &= -1.1905, & f_2 &= -2.0252, & f_3 &= -2.8404; \\ f_{-2} &= 0.26987, & f_{-3} &= 1.8957, & f_{-4} &= 2.7103. \end{aligned} \quad (13)$$

Following Henrard & Lemaître (1983), we define a dimensionless time and canonical momentum,

$$\begin{aligned} \tau &= \left| \frac{\beta\varepsilon^2}{4} \right|^{1/3} t, \\ R &= \left| \frac{2\beta}{\varepsilon} \right|^{2/3} \Phi, \end{aligned} \quad (14)$$

and a modified canonical coordinate r ,

$$\begin{aligned} r &= -\phi & \text{if } \varepsilon > 0 \\ &= \pi - \phi & \text{if } \varepsilon < 0. \end{aligned} \quad (15)$$

The new, dimensionless Hamiltonian in the canonical variables (r, R) is then given by

$$K = -3\Delta R + R^2 - 2\sqrt{2R}\cos r \quad (16)$$

where the dimensionless resonance distance Δ is

$$\Delta = \frac{(p+1)n_{\text{pl}} - pn_c}{|27\beta\varepsilon^2/4|^{1/3}}. \quad (17)$$

A few notes:

- The strength of the resonance can be parametrized by the dimensionless ratio

$$\begin{aligned} s &\equiv \frac{|27\beta\varepsilon^2/4|^{1/3}}{pn_c} \\ &= \text{sgn}(p) \left| \frac{9f_p m_{\text{pl}} a_c}{\sqrt{8|p|m_* a_{\text{pl}}}} \right|^{2/3}. \end{aligned} \quad (18)$$

Note that s is positive for interior resonances and negative for exterior ones.

- For small eccentricity, we can write $2R \simeq (e/s_e)^2$, where the eccentricity scale is

$$\begin{aligned} s_e &\equiv \frac{1}{(\mu a_c)^{1/4}} \left| \frac{\varepsilon}{2\beta} \right|^{1/3} \\ &= \left| \frac{f_p m_{\text{pl}} a_c}{3p^2 m_* a_{\text{pl}}} \right|^{1/3}. \end{aligned} \quad (19)$$

Note that

$$s_e^2 = \frac{2}{9p} s. \quad (20)$$

- As the eccentricity $e \rightarrow 0$ and the planet mass $m_{\text{pl}} \rightarrow 0$, $n_c = n$ is the unperturbed mean motion, and the ‘‘exact resonance’’ condition $pn_c = (p+1)n_{\text{pl}}$ corresponds to $\Delta = 0$.
- The topology of the phase space determined by this dimensionless resonant Hamiltonian depends only upon the value of Δ .
- The range of the resonant perturbation is $|(p+1)n_{\text{pl}} - pn_c| \sim pn_c s$. This means that the ‘‘width’’ of the resonance is proportional to $m_{\text{pl}}^{2/3}$.

The phase-space trajectories follow level curves of the dimensionless resonant Hamiltonian K (Equation 16). Figure 1 shows plots of the level curves for various values of Δ to illustrate the phase-space topology. In these plots, we use the Cartesian variables $(x, y) = \sqrt{2R}(\cos r, \sin r)$, which are also canonical (x is the momentum and y is the coordinate). Thus, the origin in these plots corresponds to zero eccentricity, and the distance from the origin is e/s_e . The phase-space structure is simple when $|\Delta| \gg 1$: the trajectories are nearly circles centered close to the origin. For $\Delta < 1$, there is only one fixed point and no homoclinic trajectory, but for $\Delta > 1$ there are three fixed points and a homoclinic trajectory exists. All the fixed points are on the x -axis; they are given by the solutions of $\partial K/\partial x = 0$ which are the real roots of the cubic equation

$$x^3 - 3\Delta x - 2 = 0. \quad (21)$$

Figure 2 plots the locations of the real roots as a function of Δ . We shall be using only the branches shown by solid lines: for $\Delta \leq 0$

$$x_1(\Delta) = (1 + \sqrt{1 - \Delta^3})^{1/3} + \Delta(1 + \sqrt{1 - \Delta^3})^{-1/3}, \quad (22)$$

and for $\Delta \geq 0$

$$x_2(\Delta) = -2\sqrt{\Delta}\cos[(\theta - 2\pi)/3], \quad \theta \equiv \cos^{-1}(-\Delta^{-1/3}). \quad (23)$$

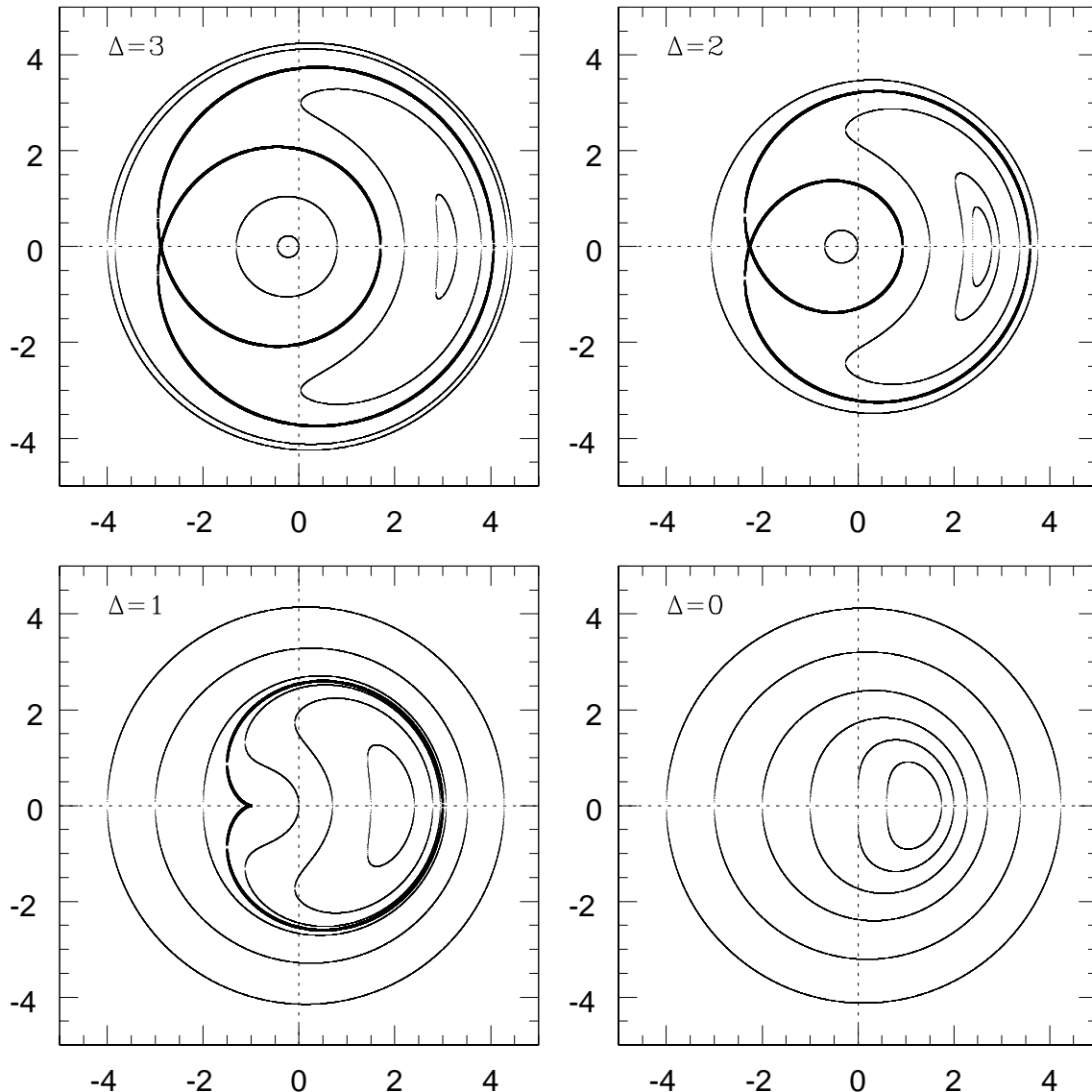


FIG. 1.— Level curves of the dimensionless resonance Hamiltonian, Equation (16), for various values of the resonance distance Δ , Equation (17). The coordinates are $(x, y) = \sqrt{2R}(\cos r, \sin r)$.

The level surface of the Hamiltonian that passes through the x_3 homoclinic point is a classical quartic curve called the limaçon of Pascal.

3. EVOLUTION OF INITIALLY CIRCULAR ORBITS IF THE PLANET MASS GROWS QUICKLY

In this section we determine the distribution of test-particle orbits that arises if the planet appears quickly. Here “quickly” means over a timescale long compared to the orbital time but short compared to the inverse of the frequency scale sn_c (Equation 18); for reference, at the 2:1 resonance of Jupiter $(sn_c)^{-1} \simeq 100$ yr. We recognize that this is probably an unrealistic model of how

most planets form, but we present it as a foil to the slow planetary growth described in the following section.

Assume that the planet mass grows suddenly from 0 to m_{pl} at time $\tau = 0$. Since the test particles have zero eccentricity at this instant, $R = 0$ so the resonance Hamiltonian $K = 0$ and the fast action $\Psi = \Lambda = (\mu a_i)^{1/2}$ where a_i is the initial semi-major axis. Then n_c is a constant of the motion that is equal to $n_i = (\mu/a_i^3)^{1/2}$, the mean motion just before $\tau = 0$ (Equation 7). The resonant mean motion is $n_{\text{res}} = (p + 1)n_{\text{pl}}/p$ and the

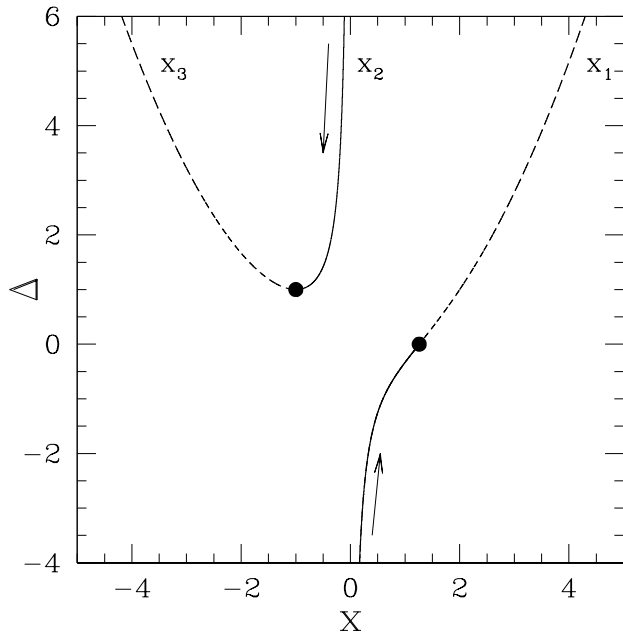


FIG. 2.— Fixed points of the dimensionless Hamiltonian, Equation (16), as a function of the resonance distance Δ . The fixed points have $r = 0, \pi$ and the variable plotted is $x = \sqrt{2R} \cos r$. The arrows indicate the evolution of initially circular orbits during the slow growth of the planet, while the dashed lines represent fixed points that are not populated by test particles during this process.

dimensionless resonance distance (Equation 17) is

$$\Delta = \frac{n_{\text{res}} - n_i}{sn_i}. \quad (24)$$

Thus a uniform initial distribution in mean motion implies a uniform distribution in Δ .

Observers more commonly work with the period ratio \mathcal{P} , defined to be greater than unity, i.e., $\mathcal{P} = n/n_{\text{pl}}$ for interior resonances and n_{pl}/n for exterior ones. Then

$$\begin{aligned} \Delta &= \frac{1}{s} \left(\frac{\mathcal{P}_{\text{res}}}{\mathcal{P}_i} - 1 \right), \quad \mathcal{P}_{\text{res}} = (p+1)/p, \quad p > 0 \\ &= \frac{1}{s} \left(\frac{\mathcal{P}_i}{\mathcal{P}_{\text{res}}} - 1 \right), \quad \mathcal{P}_{\text{res}} = p/(p+1), \quad p < -1. \end{aligned} \quad (25)$$

For $|s| \ll 1$, the effects of the resonance are only important if $|\mathcal{P}/\mathcal{P}_{\text{res}} - 1| \ll 1$ and in this case we can combine the two formulae above as

$$\Delta = \frac{1}{|s|} \left(1 - \frac{\mathcal{P}_i}{\mathcal{P}_{\text{res}}} \right). \quad (26)$$

For $\tau > 0$ the particles evolve at fixed energy K and action Ψ . For initially circular orbits, $e_i = 0$, $\Psi = \sqrt{\mu a_i}$, and the constancy of Ψ implies that $a[1 + p - p(1 - e^2)^{1/2}]^2 = a_i$ and

$$n = n_i [1 + p - p\sqrt{1 - e^2}]^3 \simeq n_i (1 + \frac{3}{2}pe^2). \quad (27)$$

Thus, the final mean motion or semi-major axis is determined by the final eccentricity e_f , and our problem is reduced to determining the distribution of eccentricities e excited by the planet. Using Equation (20), Equation

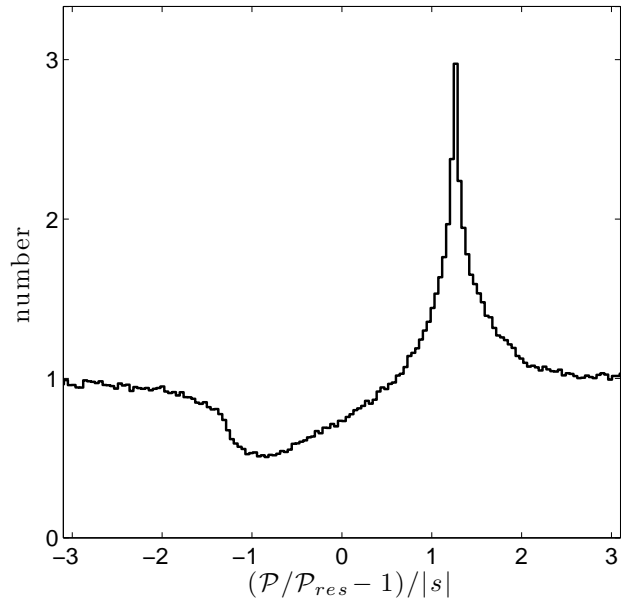


FIG. 3.— Distribution of period ratios in the vicinity of a resonance when the planet mass grows quickly, as described in §3. Period ratios are plotted in units of the resonance strength $|s|$ (Equation 18).

(27) can be simplified to

$$n = n_i \left(1 + \frac{2}{3}Rs \right). \quad (28)$$

Now suppose a particle initially has mean motion separated from the resonance by a fractional distance fs where f is of order unity, i.e., $n_i - n_{\text{res}} = fsn_i$. Then from Equation (24), $\Delta = -f$ so the resonance Hamiltonian K (eq. 16) is completely specified. The initial conditions are $x = \sqrt{2R} \cos r = 0$, $y = \sqrt{2R} \sin r = 0$, and we integrate the equations of motion $dx/d\tau = -\partial K/\partial y$, $dy/d\tau = \partial K/\partial x$ to the present time; then the present value of R determines the present mean motion in units of s through Equation (28). Thus the steady-state distribution of mean motions is the same for all resonances of this type, independent of the planet mass, the resonance integer p , whether the resonance is interior or exterior, etc., so long as the mean motions are expressed in terms of the dimensionless parameter s of Equation (18).

Using this procedure we can compute the expected distribution of mean motions near a resonance in the limiting case where the planet mass grows fast. This has been done in Figure 3, where we have chosen 10^7 particles with zero initial eccentricity and initial mean motion chosen randomly in the interval $|\mathcal{P}_i/\mathcal{P}_{\text{res}} - 1| \leq 3|s|$. Each particle has been followed for a time chosen uniformly random between 50 and 150.

We observe from Figure 3 that the distribution of particles exhibits a peak at period ratios larger than resonance, and a trough at period ratios smaller than resonance (this statement holds for both interior and exterior resonances). The shape resembles a P-Cygni profile in the context of spectroscopic emission lines. Using this analogy we can characterize the redistribution of systems close to resonances by computing the equivalent widths

(EWs) in these regions as

$$\text{EW}_{\pm} = \int_{\mathcal{P} \gtrless \mathcal{P}_{\text{res}}} \left[\frac{y_f(\mathcal{P})}{y_i} - 1 \right] d\mathcal{P}, \quad (29)$$

where y_i is the initial number of particles per unit period ratio (assumed uniform) and $y_f(\mathcal{P})$ is the final distribution. Here, the initial distribution defines our background or “continuum”. In our convention a trough (“absorption line”) has negative EW and a peak (“emission line”) has positive EW. If particles are rearranged near the resonance but do not migrate or escape the sum of the EWs should be zero. The results from the simulation in Figure 3 give

$$\text{EW}_+ = -\text{EW}_- = 0.685|s|\mathcal{P}_{\text{res}}. \quad (30)$$

4. EVOLUTION OF INITIALLY CIRCULAR ORBITS IF THE PLANET MASS GROWS SLOWLY

We now examine how initially circular orbits of test particles in the vicinity of resonance evolve as the planet mass grows gradually from small values. The slowly varying parameter is the resonance distance $\Delta \propto m_{\text{pl}}^{-2/3}$. For very small values of planet mass, $|\Delta|$ is large [for all but the measure zero case in which $(p+1)n_{\text{pl}} = pn_c$]. As the planet mass grows to its final value, $|\Delta|$ decreases.

4.1. Analysis

Provided that there is no separatrix-crossing event, an initially circular orbit of a test particle will evolve with two adiabatic invariants: $\Psi = \sqrt{\mu a}(1 + p - p\sqrt{1 - e^2})$ and $A = \oint R dr = \oint y dx$, the area enclosed by the phase trajectory in the (x, y) plane. If a separatrix crossing occurs, there is a discontinuous change in A ; this does occur for a range of parameters, as detailed below.

In the discussion below, we use subscripts i and f to denote initial and final values of parameters. For initially circular orbits, the adiabatic invariant $\Psi = \sqrt{\mu a_i}$ and the constant n_c (Equation 7) is equal to the initial mean motion n_i .

Consider first the implications of the adiabatic invariant Ψ . The relations (24) and (28) continue to hold, except that now the resonance strength s is growing slowly with time. Thus, the final mean motion or semi-major axis is determined by the final eccentricity e_f or its scaled version R_f , and our problem is reduced to determining R_f . We now show that it is possible to determine R_f from the adiabatic invariance of A for most (but not all) initially circular orbits.

For initially circular orbits, $A_i = 0$. Therefore, these orbits will adiabatically follow the evolution of the fixed point close to the origin. There are two cases to consider, one for each “side” of the resonance:

Test particle is initially wide of the resonance — This means that the test particle is further from the planet than the resonance, that is, for an interior resonance ($p > 0$) the test particle is inside the resonance and $n_i > (1+1/p)n_{\text{pl}}$, while for an exterior resonance ($p < -1$) the test particle is outside the resonance and $n_i < (1+1/p)n_{\text{pl}}$. For both cases Δ_i is negative, and large in absolute value. Initially circular orbits are near the fixed point x_1 in Figure 2. As Δ increases, these orbits evolve along the fixed point x_1 , i.e., upward along the curve labeled x_1

in the fourth quadrant of Figure 2, as indicated by the upward pointing arrow. No matter how large the planet mass grows, Δ remains negative, so the test particle can never evolve onto the dotted portion of the x_1 curve. (The point marked with a black circle at $\Delta = 0, x_1 = 2^{1/3}$ corresponds to the measure-zero case in which $n_i = (1 + 1/p)n_{\text{pl}}$.) Thus, the final orbits have a fixed eccentricity (Equation 22),

$$e_f = s_e x_1(\Delta_f) \quad \text{or} \quad R_f = \frac{1}{2} x_1^2(\Delta_f), \quad (31)$$

and a final mean motion given by Equation (28).

Test particle is initially narrow of the resonance — In this case Δ_i is large and positive and initially circular orbits are near the fixed point x_2 in Figure 2. As Δ decreases, these orbits evolve along the fixed point x_2 , i.e., downward along the inner curve in the second quadrant in Figure 2, as indicated by the downward pointing arrow.

No matter how large the planet mass grows, Δ remains positive. This branch represents the final orbits for $\Delta_f > 1$ (equivalently, $pn_i < (p+1)n_{\text{pl}} - psn_c$), and for these orbits the final eccentricity is fixed at (Equation 23)

$$e_f = s_e x_2(\Delta_f) \quad \text{or} \quad R_f = \frac{1}{2} x_2^2(\Delta_f). \quad (32)$$

A complication in this case is that the fixed point x_2 vanishes at $\Delta = 1$, i.e., for $pn_i = (p+1)n_{\text{pl}} - psn_c$ where s is the resonance strength defined by (18). For $0 < \Delta_f < 1$ [i.e., $(p+1)n_{\text{pl}} - psn_c < pn_i < (p+1)n_{\text{pl}}$], the adiabatic evolution leads the trajectory to coincide with the separatrix when $\Delta = 1$. There ensues a discontinuous increase in the value of A , which jumps from $A = A_i = 0$ to $A = 6\pi$ (which is the area enclosed by the separatrix at $\Delta = 1$). After this jump A is again an adiabatic invariant so its final value is $A_f = 6\pi$. The final orbits in these cases are not described by a stationary value of the eccentricity, because the trajectory in the (x, y) plane is neither a fixed point nor a circle centered at the origin. Similarly, the final mean motion is not fixed. An approximate estimate of the mean final eccentricity is

$$\langle e \rangle_f = s_e \sqrt{A_f/\pi} = \sqrt{6} s_e, \quad (33)$$

but to determine the final distribution of eccentricities and mean motions in this region it is simpler to integrate the equations of motion in the resonance Hamiltonian K (see the following subsection).

Combining Equations (28), (31), and (32), the final mean motion of particles that do not cross the separatrix is

$$\begin{aligned} n &= n_i \left(1 + \frac{1}{3} s x_1^2 \left[\frac{(n_{\text{res}} - n_i)}{s n_i} \right] \right), & p(n_{\text{res}} - n_i) > 0, \\ &= n_i \left(1 + \frac{1}{3} s x_2^2 \left[\frac{(n_{\text{res}} - n_i)}{s n_i} \right] \right), & p[n_{\text{res}} - (1 + s)n_i] > 0, \end{aligned} \quad (34)$$

where n_i is the initial mean motion, and the characteristic resonance strength s (Equation 18) is evaluated for the final planet mass m_{pl} . If the initial distribution in mean motion is uniform, the final density of the mean-motion distribution is given by

$$dN(n) \propto dn_i = \frac{dn_i}{dn}, \quad (35)$$

which is easily evaluated numerically from Equation (34)—see Figure 4.

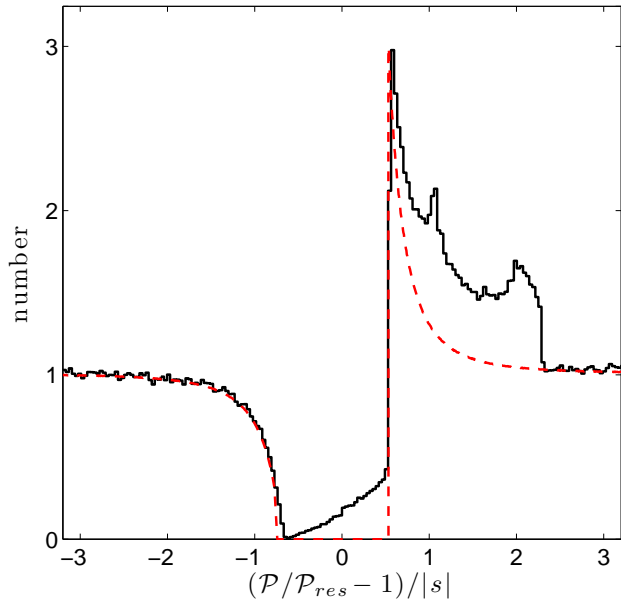


FIG. 4.— Distribution of period ratios in the vicinity of a resonance when the planet mass grows slowly, as described in §4. Period ratios are plotted in units of the resonance strength $|s|$ (Equation 18). The red dashed curves show the expected distribution for particles that do not cross the separatrix, as given by Equations (34) and (35).

For these particles there is a gap in the distribution of final mean motions,

$$\begin{aligned} n_{\text{res}}(1 - \frac{2}{3}|s|) < n < n_{\text{res}}(1 + \frac{2^{2/3}}{3}|s|), \quad p, s > 0, \\ n_{\text{res}}(1 - \frac{2^{2/3}}{3}|s|) < n < n_{\text{res}}(1 + \frac{2}{3}|s|) \quad p, s < 0. \end{aligned} \quad (36)$$

Note that the gap is not symmetric about the exact resonance value, $n_{\text{res}} = (p+1)n_{\text{pl}}/p$. The size of the gap is

$$\Delta n_{\text{gap}} = 2.587(p+1) \left| \frac{m_{\text{pl}}}{m_*} \frac{a_c f_p}{a_{\text{pl}} p^2} \right|^{2/3} n_{\text{pl}}. \quad (37)$$

The particles that cross the separatrix have librating eccentricities and mean motions; as we show below, these particles partially fill the gap and also broaden the peak wide of resonance.

4.2. Numerics

For our numerical experiments, we assume that the planet mass varies as

$$m_{\text{pl}}(t) = m_{p,f} \tanh t/t_{\text{pl}}. \quad (38)$$

The timescale t_{pl} can be thought of as the formation time of the planet. In simulations with $t_{\text{pl}} = 0$ the planet forms suddenly, i.e., the integration is started with the final planet mass m_{pl} .

We follow the evolution induced by the resonance Hamiltonian K for a large number of test particles on initially circular orbits, uniformly distributed in mean motion. We start the integrations at a time when the planet mass $m_{\text{pl},i} = 10^{-6}m_{\text{pl},f}$, which means that the initial characteristic frequency $s_i = 10^{-4}s_f$. Thus for

any particle the final resonance distance $\Delta_f = 10^{-4}\Delta_i$; we shall follow particles with $|\Delta_f| \leq 3$ which implies that the initial distribution should be chosen uniform in Δ_i between $\pm 3 \times 10^4$. We use a growth time $t_{\text{pl}} = 100$ and follow the particles for a time chosen uniformly random between 250 and 750; we have checked that the results are insensitive to these choices. The resulting distribution of mean motions is shown in Figure 4; as expected, the distribution mostly agrees with the distribution derived analytically in the preceding subsection, but the particles that have crossed the separatrix partially fill in the resonance gap (Equation 36) and enhance the peak to the right of it.

The equivalent widths are

$$EW_+ = -EW_- = 0.956|s|\mathcal{P}_{\text{res}}, \quad (39)$$

almost 50% larger than the result when the planet grows fast (Equation 30).

5. NUMERICAL INTEGRATIONS OF THE RESTRICTED THREE-BODY PROBLEM

We ran numerical experiments to follow the motion of test particles subject to gravitational forces from the central star and an orbiting massive planet. We work in the astrometric reference frame, in which the equations of motion for a test particle can be written as

$$\frac{1}{n_{\text{pl}}^2} \frac{d^2 \vec{x}}{dt^2} = -\mu_1 \frac{\vec{x}}{|\vec{x}|^3} - \mu_2 \left[\frac{\vec{x} - \vec{x}_{\text{pl}}(t)}{|\vec{x} - \vec{x}_{\text{pl}}(t)|^3} + \frac{\vec{x}_{\text{pl}}(t)}{|\vec{x}_{\text{pl}}(t)|^3} \right] \quad (40)$$

where $\mu_1 = m_*/(m_* + m_{\text{pl}})$ and $\mu_2 = 1 - \mu_1 = m_{\text{pl}}/(m_* + m_{\text{pl}})$. As usual a_{pl} and $n_{\text{pl}}^2 = G(m_* + m_{\text{pl}})/a_{\text{pl}}^3$ are the semi-major axis and squared orbital frequency of the planet. The positions of the test particle \vec{x} and the massive planet \vec{x}_{pl} are normalized by a_{pl} . Times are given in planet years, $2\pi/n_{\text{pl}}$.

In these simulations the planet mass m_{pl} or μ_2 is initially zero and grows during the simulation according to the formula (38). During this growth the planetary semi-major axis a_{pl} is kept constant, although there are other plausible choices, e.g., $a_{\text{pl}} \propto (m_* + m_{\text{pl}})^{-1}$, as would be expected if the planet gained mass isotropically.

If the planet eccentricity e_{pl} is zero and the growth of the planet mass is sufficiently fast or slow, the results of these simulations should be directly comparable to the analytic results we obtained in §3 and §4.

5.1. Initial conditions

We typically consider planet masses m_{pl} in the range 10^{-4} – $10^{-3}m_*$, or 0.1–1 Jupiter mass for a solar-mass host star. For comparison most *Kepler* planets have masses between 0.01 and 0.1 Jupiter masses, and most planets discovered by radial-velocity measurements have masses between 0.1 and 10 Jupiter masses.

We assume for simplicity that the test particle is inside the massive planet, i.e., we consider interior resonances only. This is a plausible simplification: inner planets are usually smaller than outer planets in the *Kepler* and radial-velocity samples because planets with smaller semi-major axes are easier to detect.

The semi-major axes a of the test particle and planet are determined using a fitting function for the probability distribution of semi-major axes in the *Kepler*

sample, after accounting for geometric selection effects (Tremaine & Dong 2011):

$$dp(a) = 0.656 \frac{(a/a_0)^{3.1}}{1 + (a/a_0)^{3.6}} \frac{da}{a}, \quad a < 1.15 \text{ AU} \quad (41)$$

where $a_0 = 0.085$ AU. We then generate an initial distribution in the period ratio \mathcal{P} ($\mathcal{P} > 1$) of a two-planet system by generating two random variables, a_1 and a_2 , from this probability distribution and computing $\mathcal{P} = \max\{(a_1/a_2)^{3/2}, (a_2/a_1)^{3/2}\}$. This procedure generates a smooth initial distribution in period ratio. For the numerical integrations, we set the semi-major axis of the massive planet to unity and the semi-major axis of the test particle is then $\mathcal{P}^{-2/3}$.

In some simulations the test particles have non-zero eccentricities e and/or inclinations i . These are assumed to be randomly distributed following a Rayleigh law,

$$dp = \frac{x dx}{\sigma_x^2} \exp(-\frac{1}{2}x^2/\sigma_x^2), \quad (42)$$

where $x = e$ or i and σ_x is an input parameter that is related to the mean and rms eccentricity or inclination by $\langle x \rangle = \sqrt{\pi/2}\sigma_x = 1.253\sigma_x$, $\langle x^2 \rangle^{1/2} = \sqrt{2}\sigma_x = 1.414\sigma_x$.

We treat the planet and host star as point particles, i.e., we do not account for possible collisions of the test particles with either body.

5.2. Numerical results and comparison with analytic theory

We start by considering two simple fiducial models to compare with our previous theoretical results. First, we consider a model for a slowly growing planet mass, which contains 10^4 test particles and has planet-formation timescale $t_{\text{pl}} = 10^4 [2\pi/n_{\text{pl}}]$ (or 10^4 orbits of the exterior planet). Second, we consider a model for a rapidly growing planet mass, which contains 2×10^4 test particles and starts with the final planet mass, i.e., $t_{\text{pl}} = 0$. Both models have a final planet mass $m_{\text{pl}} = 0.001m_*$ (1 Jupiter mass), a planet eccentricity $e_{\text{pl}} = 0$, and zero eccentricities and inclinations for the test particles (i.e., $\sigma_e = \sigma_i = 0$ in Equation 42). The initial distribution of semi-major axes or periods of the test particles is obtained using the procedure in §5.1, with the period ratio restricted to the range $1.3 \leq \mathcal{P} \leq 2.5$.

In the simulation for the slow case, $\approx 4\%$ of the test particles were lost to escape orbits, mostly from orbits initially near the planet with $\mathcal{P}_i \lesssim 4/3$, while for the fast case the same happens for $\approx 10\%$ of the test particles, almost all from orbits with $\mathcal{P}_i \lesssim 7/5$.

5.2.1. Final eccentricity

In Figure 5, we compare our numerical results for the final eccentricity as a function of the initial period ratio with those obtained from the analytic formalism of §4 for a slowly growing mass planet. As expected, substantial eccentricities are excited in orbits that start close to the first-order (4:3, 3:2 and 2:1) resonances. The eccentricities are also excited in smaller ranges around the second-order (7:5 and 5:3) resonances, a result that is not captured by our simple analytic theory. Analytic curves for the 3:2 and 2:1 resonances (blue and red, respectively, from Equations 34 and 35) are plotted for

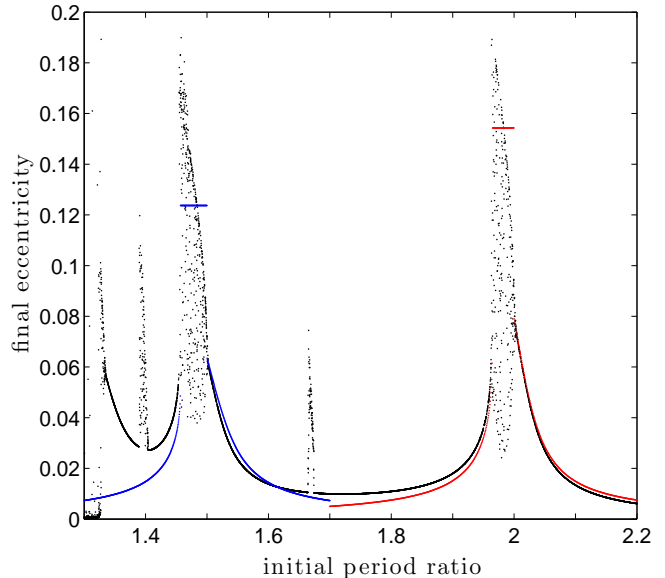


FIG. 5.— Final eccentricity as a function of the initial period ratio n_i/n_{pl} for a simulation with 10^4 test particles and parameters $m_{\text{pl}} = 0.001m_*$, $t_{\text{pl}} = 10^4$, $e_{\text{pl}} = 0$, and $\sigma_e = 0$. Results are shown after 5×10^4 planet orbits. The blue and red lines indicate the analytic results for a slowly growing planet, for the 3:2 and 2:1 resonances, respectively. The analytic results are only shown for particles that do not cross the resonance separatrix, since particles that do cross have librating eccentricities (these produce the elongated ovals filled with scattered points). The horizontal lines denote the approximate analytic prediction for the mean eccentricity of particles with oscillating eccentricity (Equation [33]).

orbits that do not cross the resonant separatrix, since these have stationary forced eccentricity (compare the red dashed lines in Figure 4). The analytic curves agree quite well with the simulations close to the resonances. The deviations grow as we move away from the resonances, since the approximation of a single resonance becomes less and less accurate. For orbits that do cross the separatrix, the figure shows an approximate estimate for the mean eccentricity from Equation (33) as a horizontal line; the extent of this line marks the range of period ratios corresponding to such orbits, from Equation (36). In this snapshot of the simulation, the regions in which the forced eccentricity oscillates are marked by clouds of points; the widths of these clouds agree reasonably well with the analytic theory, although the theoretical estimates of the mean eccentricities, marked by horizontal red and blue bars, are somewhat too high.

For the case when the planet mass grows quickly the final eccentricity is never stationary: it oscillates between zero and a maximum value similar to that in Figure 5. The results obtained from the resonance Hamiltonian integration in §3 agree quite well with the numerical simulations. Near the 2:1 and 3:2 resonances, both produce a similar cloud of final eccentricities for a given initial period ratio.

5.2.2. Period-ratio distribution

In Figure 6 we show the distribution in period ratio for the test particles in the fiducial simulations. The upper and lower panels show the results for the slowly and fast growing mass cases, respectively. We also plot in red lines the probability density function (PDF) around the first-order resonances, as computed in §3 and §4.2 respectively

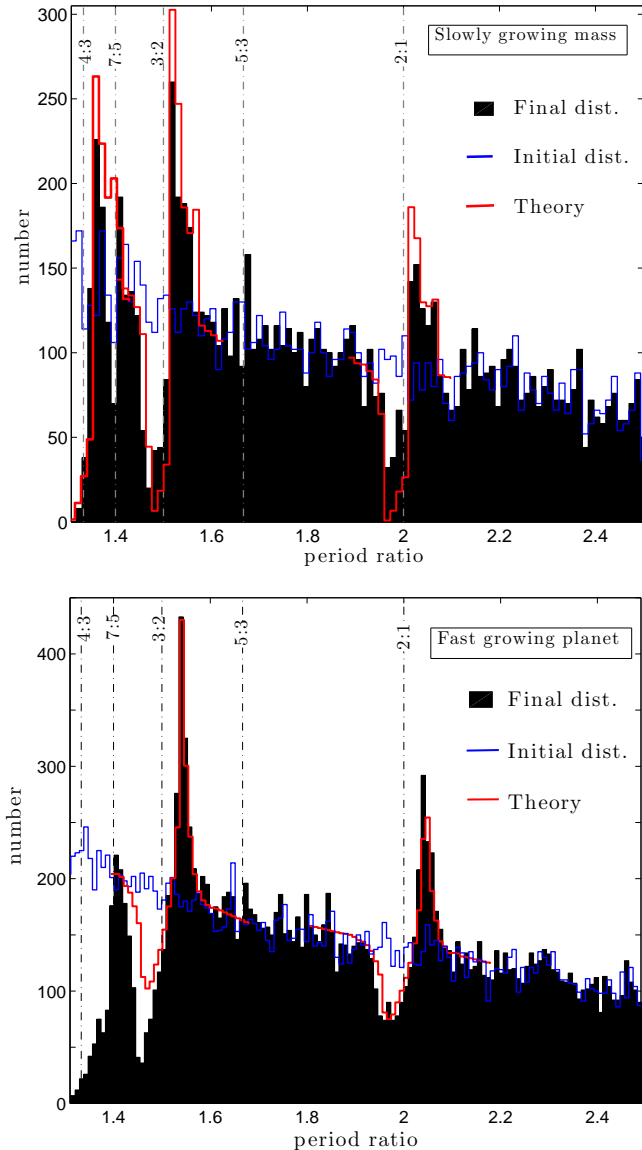


FIG. 6.— Number density of test particles as a function of the period ratio \mathcal{P} (black histograms), for the fiducial three-body integrations with parameters $m_{\text{pl}} = 0.001m_*$, $e_{\text{pl}} = 0$, $\sigma_e = 0$, and $\sigma_i = 0$. The initial distribution in period ratio is given by Equation (41) and shown by blue lines. The upper panel shows the distribution after 5×10^4 planet years for a simulation with growth time $t_{\text{pl}} = 10^4$ planet years, as well as the theoretical PDF around the 4:3, 3:2, and 2:1 resonances, shown in red lines. The latter distribution is obtained as in §4.2 (see Figure 4) and rescaled to the number of systems in the three-body integrations. The lower panel shows the same for a set of three-body integrations in which the growth time $t_{\text{pl}} = 0$; in this panel the theoretical PDF is obtained as in §3 (see Figure 3).

(see black lines in figure 3 and 4), scaling our results to the mean number of initial planets in the simulation as expected from the background distribution in Equation (41).

As predicted by the analysis for a slowly growing planet in §4, there is a peak in the number of planetary systems at period ratios slightly larger than the exact resonances and a deficit at period ratios smaller than the resonance position. The strongest enhancements are at the first-order 4:3, 3:2, and 2:1 resonances, but the effect is

TABLE 1
EQUIVALENT WIDTHS AROUND RESONANCES

Resonance	EW_+	EW_-	$ EW_{\pm} $ from Equation (39)
4:3	0.0073 ^a	-0.034	0.033
7:5	0.0043	-0.0051	—
3:2	0.033	-0.034	0.033
5:3	0.0033	-0.0036	—
2:1	0.030	-0.030	0.034

NOTE. — Equivalent widths (Equation 29) from three-body integrations, for slow growth of the planet mass.

^a Note that 82% of the test particles around 4:3 are lost to escape orbits and this decreases the value of EW_+ , while slightly increasing the absolute value of EW_- .

also weakly visible at the second-order 7:5 and 5:3 resonances. Note, however, that the 7:5 resonance is close enough to 4:3 that the assumption of an isolated resonance used in the theory is suspect. Similarly, the 4:3 resonance is close enough to the planet that a significant fraction of the particles at smaller period ratios are ejected by the planet.

The features seen in the three-body integrations at the first-order resonances are roughly consistent with the predictions of §4 (red lines in Figure 6)). Specifically, the theory is able to reproduce reasonably well the position and height of the peaks and the width and depth of the gaps at the 3:2 and 2:1 resonances.

Similarly, as seen in the lower panel of Figure 6, the theory of §3 for the rapidly growing planet agrees reasonably well with the simulations around the 3:2 and 2:1 resonances. We observe, however, that the gap narrow of the 3:2 resonance is deeper than the single-resonance theory predicts, which is mainly due to a fraction of the particles that are excited to high eccentricities ($e \simeq 0.2-0.6$) and larger period ratios (310 particles with initial period ratio $1.4 < \mathcal{P}_i < 1.5$ have a final period ratio $1.6 < \mathcal{P} < 2.5$, while 16 are ejected from the system). The agreement with the single-resonance approximation is even worse closer to the planet: in fact, this approximation breaks down completely when first-order resonances overlap, which is expected for period ratios < 1.33 for a Jupiter-mass planet (Wisdom 1980). Additional discrepancies arise from ejection of test particles by the planet, which occurs for 77% of the particles with $\mathcal{P}_i < 7/5$.

In summary, the single-resonance analysis of §3 and §4 is able to reproduce the main features of the three-body integrations around the 3:2 and 2:1 resonances. The period-ratio distributions for both slow and fast planet growth exhibit peaks wide of the resonance (period ratios larger than the resonance value) and troughs or gaps narrow of the resonance. This result suggests that a broad range of planet-formation processes on intermediate timescales will produce a similar period-ratio distribution, so long as the planet does not migrate. However, the distributions differ in detail when the planet mass is increased slowly or fast. Specifically, the slow case produces both peaks and troughs that are sharper and lie closer to the resonance.

5.2.3. Equivalent widths around resonances

The equivalent widths measured from the fiducial simulation of a slowly growing planet are shown in Table 1,

along with the predictions from Equation (39). In most cases the EWs on either side of the resonances are almost equal and opposite, confirming that the resonances lead to shuffling of the test particle semi-major axes but not any overall loss or accumulation.

As expected, the largest EWs are at the 3:2 and 2:1 resonances, $\simeq 0.033$ and $\simeq 0.030$, respectively. The EWs at 3:2 and 2:1 agree with the single-resonance approximations (Equation 29). The 4:3 resonance agrees less well because 182 test particles around this resonance were ejected. But even in this case the single-resonance theory matches at least the width of the trough, EW_- .

For the fast mass increase case, we measure $EW_- = -0.0262$ and $EW_+ = 0.0254$ around the 2:1 resonance, and the single-resonance theory (Equation 30) yields $|EW_{\pm}| = 0.0244$, in reasonably good agreement. At the 3:2 resonance, $EW_- = -0.037$ and $EW_+ = 0.030$, while the single-resonance theory predicts $|EW_{\pm}| = 0.0237$. Here the difference between the single-resonance theory and the three-body integrations is mostly due to the excitation of somewhat larger eccentricities in the integrations that tend to populate the peak wide of 3:2 with more particles, while excavating a deeper gap around this resonance; 310 test particles with $1.4 < \mathcal{P}_i < 1.5$ are promoted to orbits with $\mathcal{P} > 1.6$ and 16 to escape orbits, which accounts for the difference in magnitude between EW_- and EW_+ . We have checked that reducing the mass of the perturber improves the agreement between the single-resonance theory and the integrations.

5.3. Dependence on input parameters

All of the simulations described so far consider a Jupiter-mass planet with zero eccentricity and test particles in initially circular and coplanar orbits, so that a direct comparison with the single-resonance theory can be made. Here we comment on how the distributions in period ratio are affected by different values of the planet mass and eccentricity, and the initial rms eccentricity and inclination of the test particles.

5.3.1. Varying the planet mass m_{pl}

We have run sets of three-body integrations in which the mass of the planet varies over the range 10^{-4} – $10^{-3}m_*$. These experiments show that the integration results obey the scalings predicted by the single-resonance theory: in particular the eccentricity of the test particles scales as $s_e \propto m_{\text{pl}}^{1/3}$, while the equivalent width varies as $|EW_{\pm}| \propto s \propto m_{\text{pl}}^{2/3}$. Thus, varying the planet mass simply produces re-scaled versions of the PDF around the 3:2 and 2:1 resonances shown in Figure 6.

These scalings are more difficult to study for resonances that are closer to the planet, both because of particle ejections and possible resonance overlap. Nevertheless, in most cases the analytical single-resonance theory allows us to scale predictions for the distribution of period ratios to different resonances and different planetary masses.

5.3.2. Varying the eccentricities: e_{pl} and σ_e

Varying the eccentricities of the test particles can strongly modify the final distribution of period ratios. In particular, values of σ_e (Equation 42) that are larger

than the eccentricity scale s_e (Equation 19) tend to suppress the characteristic peak+trough or ‘‘P-Cygni’’ feature around first-order resonances. For reference, from Equation (19) the eccentricity scale for a Jupiter-mass planet at the 3:2 and 2:1 resonances is 0.05 and 0.063, respectively. For values of σ_e lower than s_e the PDFs are similar to those starting with initially circular orbits ($\sigma_e = 0$).

Non-zero eccentricity of the perturber is expected to introduce chaotic zones in the vicinity of the resonances, such that initially circular orbits are excited to higher eccentricity over a wider range in period ratios compared with the case of a zero-eccentricity perturber. In numerical simulations with perturber eccentricities $e_{\text{pl}} = 0.05$ – 0.1 , we observe that a large fraction of test particles with $\mathcal{P}_i < 3/2$ are ejected to escape orbits, leaving a strong gap around 3:2 and almost no evidence of a peak wide of the resonance. Additionally, the gap around the 2:1 resonance is observed to be wider and less deep than for a zero-eccentricity perturber, while the peak wide of the resonance is observed to be somewhat weaker. Non-zero eccentricities could also lead to slow evolution of the period-ratio distribution on timescales much longer than the 10^4 planet orbits used in the fiducial simulations; we have carried out extended integrations for up to 10^5 planet orbits but see no additional changes in the period-ratio distribution. In summary, the non-zero eccentricity of the perturber tends to smear out the characteristic ‘‘P-Cygni’’ profile that we observe in the zero-eccentricity simulations.

5.3.3. Varying the inclinations: σ_i

We have run three-body integrations with parameters $\sigma_e = 0.01$ and $\sigma_i = 0.1$. The latter parameter gives a mean inclination of $\langle i \rangle \approx 7^\circ$, a value that is somewhat higher than estimates of the mean inclinations in *Kepler* multi-planet systems: $< 5^\circ$ (Tremaine & Dong 2011) or 1.0° – 2.3° (Fabrycky et al. 2012). Although the dominant features around the first-order 3:2 and 2:1 resonances are still present, the ‘‘P-Cygni’’ profile shows a less sharp peak that is shifted to larger period ratios, and gaps that are slightly wider than in the zero-inclination case. More specifically, we find that at 2:1 the equivalent widths slightly increase to $|EW_{\pm}| = 0.033$ (see values in Table 1 for comparison with the fiducial simulation), while at 3:2 we observe that more particles are ejected to escape orbits relative to the zero-inclination case, resulting in an increase in magnitude of EW_- to -0.038 and a decrease of EW_+ to 0.021. Finally, the gap at the second-order 7:5 resonance gets wider by a factor of roughly two.

6. COMPARISON WITH THE *KEPLER* SYSTEMS

We now compare our results with the *Kepler* catalog of 242 two-planet systems as obtained from Fabrycky et al. (2012). We do not consider systems with more than two planets since we have not investigated three-body resonances in this paper. We also compare with the 33 two-planet systems discovered by radial velocity (RV) observations, using the *The Exoplanet Orbit Database* as of September 2012 (Wright et al. 2011). We limit our analysis to a range in period ratio \mathcal{P} of 1.3–2.5, in which the first-order resonances are 2:1, 3:2, and 4:3. After this cut our sample is reduced to 116 and 10 two-planet systems from the *Kepler* and RV catalogs, respectively.

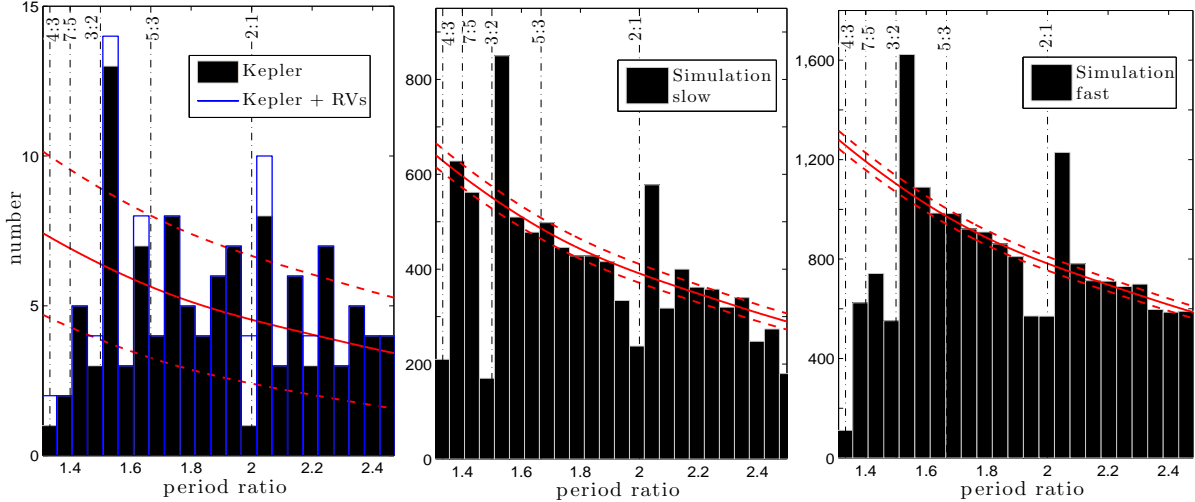


FIG. 7.— Number density of systems as a function of the period ratio. The left panel shows the *Kepler* sample (black histogram) and the *Kepler* sample plus the RV sample (blue line). The middle and right panels show the results of the fiducial simulations for a slowly and rapidly growing planet, respectively. The solid red lines indicate the initial distribution in period ratio given by Equation (41), scaled to the number of systems in each panel (ignoring the small RV contribution in the left panel) and the red dashed lines its $1-\sigma$ error bands. The vertical dot-dashed lines show the positions of the first- and second-order resonances. All histograms have the same binning of 0.05.

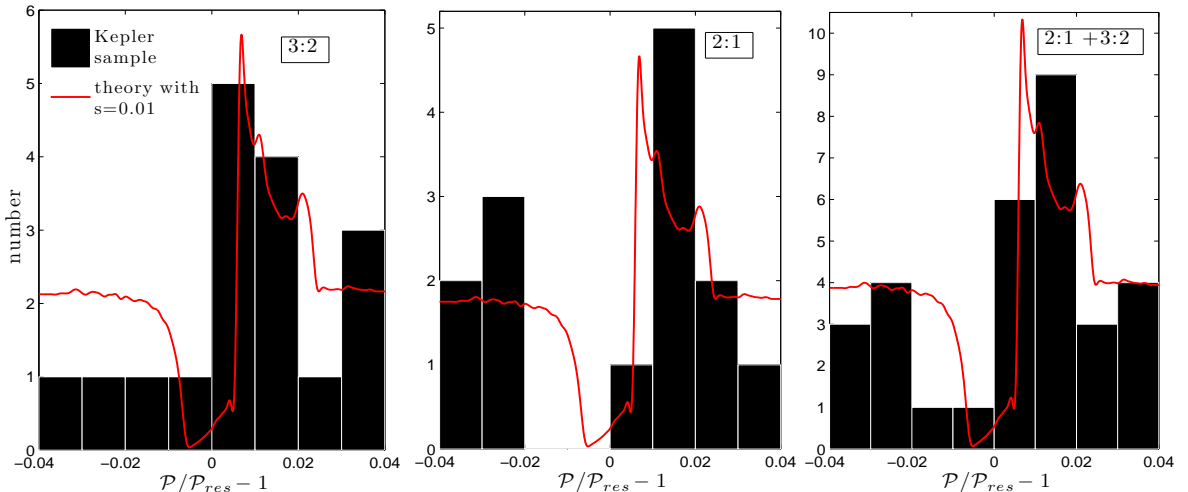


FIG. 8.— Distribution in period ratio of the *Kepler* two-planet systems near the 3:2 and 2:1 resonances (left and middle panels). In the right panel the two distributions are added together (for given values of the shifted and normalized period ratio $\mathcal{P}/\mathcal{P}_{res} - 1$). The red line indicates the theoretical distribution for a slowly growing planet (the same as in Figure 4) with a strength parameter (Equation 18) $s = 0.01$, normalized to the number of *Kepler* planets in each panel.

In Figure 7, we show the distribution of period ratios for the observations (left panel) and the fiducial simulations. We also show the expected initial distribution of period ratios as determined by the algorithm described in the paragraph containing Equation (41), along with its $1-\sigma$ confidence limits to suggest whether peaks and dips are significant.

The observations exhibit statistically significant peaks just outside (larger \mathcal{P} than) the 3:2 and 2:1 resonances, although the peak at 2:1 only exceeds $1.5-\sigma$ significance when the RV planets are included in the sample (these statements depend on the binning, which has been chosen to maximize the significance of the near-resonant fea-

tures). The observations show troughs narrow of the 3:2 and 2:1 resonance, although these are only marginally significant ($1-1.5\sigma$). There is also a deficit of systems with period ratios $\mathcal{P} \lesssim 1.4$; this likely arises from the depletion of planets that suffer close encounters and are scattered onto collision or ejection orbits. There are no statistically significant features at any second-order resonance. Therefore, we will concentrate our analysis on the first-order 2:1 and 3:2 resonances.

6.1. The 3:2 and 2:1 resonances

As pointed out by Lissauer et al. (2011b) and Fabrycky et al. (2012) and also shown in Figure 7,

two-planet systems close to the 3:2 and 2:1 resonances prefer period ratios wide of the resonance within a few percent; in particular, the data show significant peaks wide of the resonances and perhaps a trough narrow of the resonance in the case of the 2:1 resonance. Here we compare the distribution of planetary systems around the 3:2 and 2:1 resonances with our simple models to test whether they are consistent.

Hereafter we shall concentrate on the more realistic model in which the mass grows slowly and will refer to the distribution obtained using the single-resonance approximation (§4 and Figure 4) as our theoretical PDF.

In Figure 8 we show the distribution of systems as a function of the shifted and normalized period ratio $\mathcal{P}/\mathcal{P}_{\text{res}} - 1$. Positive and negative values of this variable lie wide or narrow of the resonance, respectively. For comparison, we show our theoretical PDF normalized to the number of planets in each panel. Here we just consider one value of the strength, $s = 0.01$, which is equivalent to a planet mass $m_{\text{pl}} \simeq 0.3M_J$ or $m_{\text{pl}} \simeq 0.4M_J$ at 3:2 and 2:1, respectively. The corresponding equivalent width is $EW_{\pm} = \pm 0.00956 \mathcal{P}_{\text{res}}$ (see Equation 39).

We observe in the left panel of Figure 8 that the theoretical PDF produces a peak similar in height and location to that observed in the *Kepler* sample around the 3:2 resonance, but the *Kepler* sample shows no sign of the expected gap. In contrast, in the middle panel the gap inside the 2:1 resonance seems to be larger in the *Kepler* observations than in the theoretical PDF. Finally, in the right panel where we add the 3:2 and 2:1 resonances together, the overall shape of the period distribution seems to agree, at least visually, with that of the theoretical PDF. More quantitative comparison requires statistical tests, to which we now turn.

6.1.1. K-S test

We use a Kolmogorov-Smirnov test (K-S test) to determine the probability that the observed sample is drawn from the same distribution as our theoretical distribution. Since we have found that the PDF obtained from the single-resonance model is a good approximation to the PDF obtained from three-body integrations starting with low-eccentricity, low-inclination orbits, we shall use the single-resonance predictions for the subsequent analysis.

Note that the *Kepler* sample contains planets with a wide range of masses. Thus we are fitting the data to some loosely defined “typical” value of the planet mass m_{pl} or dimensionless resonance strength s (Equation 18).

In Figure 9 we show the p -values obtained from the K-S test for the *Kepler* planets near the 3:2 and 2:1 resonances, and for the sum of these two distributions at given $\mathcal{P}/\mathcal{P}_{\text{res}} - 1$ (from top to bottom panels). For reference, we also show the p -value obtained by comparing the *Kepler* planets to a uniform distribution (horizontal dashed line). In this test, we have restricted the samples to the range $|\mathcal{P}/\mathcal{P}_{\text{res}} - 1| < 0.04$. We have experimented with other ranges between 0.03 and 0.1 and found that 0.04 provides the most stringent comparisons. For ranges larger than 0.04 there are too many particles far from resonance that dilute the signal; also the test becomes biased by large-scale gradients in the period ratio distribution. For ranges smaller than 0.03 there are too few planets left in the sample.

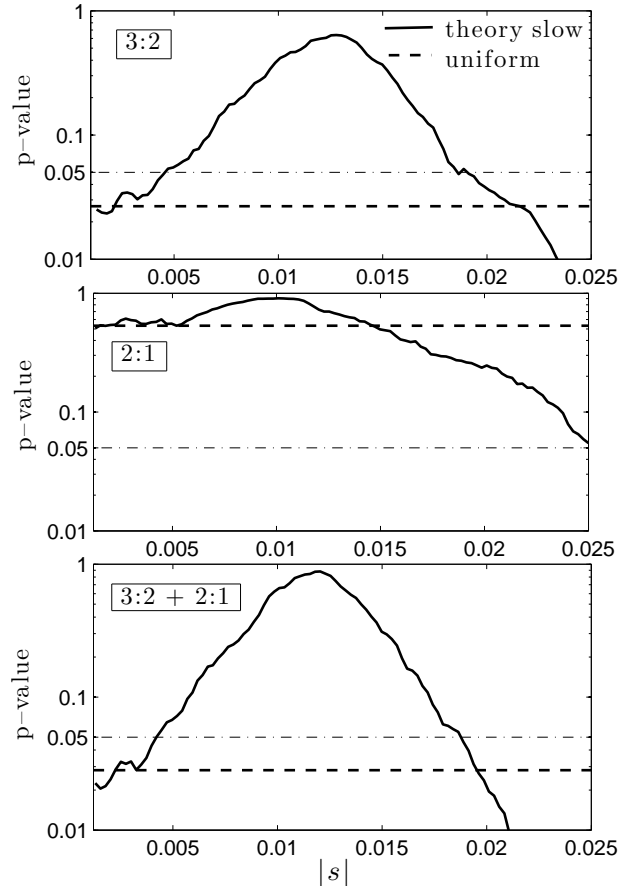


FIG. 9.— p -values as a function of the resonance strength s (Equation 18) obtained from a Kolmogorov-Smirnov test comparing the *Kepler* two-planet sample with the theoretical PDF for a slowly growing planet that does not migrate (solid line). The horizontal dashed line represents a uniform density distribution, and the dash-dot line represents a significance level $p = 0.05$ —models below this line are excluded at the 95% confidence level. We limit the test to the range $|\mathcal{P}/\mathcal{P}_{\text{res}} - 1| < 0.04$ to maximize its power.

As usual, if the p -value is below a given value α there is a probability of $1 - \alpha$ that the *Kepler* data are not drawn from the PDF predicted by the single-resonance model. Thus, in each panel we add a horizontal dot-dashed line at 0.05 to discriminate between models at the 95% confidence level. The middle panel of Figure 8 shows that there is no statistically significant signal at the 2:1 resonance, in the sense that a uniform distribution of period ratios is consistent with the data (at $p = 0.53$). This result does not exclude the possibility that a significant signal would be revealed by some other more sensitive test. In the top and bottom panels, there is a significant signal in that the uniform distribution is excluded at about the 97% confidence level.

These results differ from those of Fabrycky et al. (2012), who find significant evidence that the distribution in period ratios around the 3:2 and 2:1 resonances are not drawn from a smooth distribution ($p = 0.0046$ and 0.029, respectively), both more than an order of magnitude smaller than our p -values. We attribute this difference mainly to our restricted data set: we use only two-planet systems whereas Fabrycky et al. use all planet pairs in multi-planet systems, so our sample is ~ 3 times smaller. The difference might also hint that near-

resonant features are more common in multi-planet systems than in two-planet systems.

7. DISCUSSION

The few hundred multiple planet candidates discovered by the *Kepler* spacecraft provide a unique window into how planets form and evolve, although we do not yet know how to interpret the limited view that we have through this window. This paper is focused on the distribution of planets near mean-motion resonances in multi-planet systems, which has two important features.

First, the number of systems near mean-motion resonances is small: the left panel of Figure 7 shows that the only resonance feature that is significant at more than the $1.5\text{-}\sigma$ level is the peak at the 3:2 resonance. As discussed in §1, this result is striking because since planet migration is believed to be a common process, and capture into a first-order resonance during convergent migration is certain if the eccentricities and inclinations of the planet pair are sufficiently small and migration is sufficiently slow when the resonance is crossed.

Second, at both the 3:2 and 2:1 first-order resonances the peak in the period-ratio distribution appears just wide of the resonance (i.e., at period ratios greater than the resonance value, if the period ratio is defined to be > 1), rather than at the resonance. In addition, the 2:1 resonance appears to have a trough in the period-ratio distribution just narrow of the resonance, although the statistical significance of the trough is weak. All of these features were pointed out already by Fabrycky et al. (2012).

Given these findings, it is natural to ask what distribution of period ratios should be expected near resonance if there is no migration, i.e., if planets form *in situ*. We have investigated two extreme limits of this process, in which the planet forms fast or slowly (relative to the characteristic dynamical time associated with the resonance). We find that in both cases the distribution of test particles near resonance develops a shape characterized by a peak wide of the resonance (period $\mathcal{P} > \mathcal{P}_{\text{res}}$ where the period ratio at resonance $\mathcal{P}_{\text{res}} > 1$) and a trough narrow of the resonance (see Figures 3 and 4). The peak and trough result from a redistribution of particles from period ratios $\mathcal{P} \lesssim \mathcal{P}_{\text{res}}$ to $\mathcal{P} \gtrsim \mathcal{P}_{\text{res}}$, rather than from an overall gain or loss of particles as would occur through processes such as ejection or migration.

7.1. Planet masses in the *Kepler* sample

The mean and median radius for the planets in the 242 two-planet systems in Fabrycky et al. (2012) are $2.46R_{\oplus}$ and $2.17R_{\oplus}$, respectively. To compare our models to the data, i.e., to estimate the strength parameter s in Figure 9, we need the mass-radius relation for the *Kepler* planets.

(i) Fitting to the planets in the solar system, Fabrycky et al. (2012) find $M = M_{\oplus}(R/R_{\oplus})^{2.06}$ for $R > R_{\oplus}$, which yields $M = 6.4M_{\oplus}$ and $4.9M_{\oplus}$ for the mean and median mass in the *Kepler* two-planet sample. (ii) From a statistical fit to transit timing variations in the *Kepler* sample, Wu & Lithwick (2012) find $M = 3M_{\oplus}(R/R_{\oplus})$, which implies $7.4M_{\oplus}$ and $6.5M_{\oplus}$ for the mean and median mass. (iii) There are four planets with measurements of both mass and radius in the radius range $2\text{--}3R_{\oplus}$; these have mean and median masses of

$7.0M_{\oplus}$ and $6.1M_{\oplus}$. All three of these crude approaches suggest a typical planet mass of about $6\text{--}7M_{\oplus}$ for the *Kepler* planets.

7.2. Planet masses required to explain features in the period distribution near resonances

Our simple theoretical model, based on slow growth of the planet masses with no migration, is consistent with the data ($p > 0.1$) shown in Figure 9 for values of the strength s between 0.006 and 0.018⁶. Equation (18) gives $s = 0.023(m_{\text{pl}}/M_J)^{2/3}$ and $s = 0.0179(m_{\text{pl}}/M_J)^{2/3}$ at 3:2 and 2:1, respectively; focusing on the 3:2 resonance, which contains the strongest signal, consistency then requires $40 \lesssim m_{\text{pl}}/M_{\oplus} \lesssim 220$. Our calculations are for a system containing a test particle and a planet of mass m_{pl} ; in the *Kepler* two-planet systems both planets have non-zero mass and in the absence of a detailed numerical study of this case the most appropriate choice is probably to identify m_{pl} in these formulae with twice the mean planet mass. Thus the mean planet mass required to explain the resonant structure seen in the *Kepler* data at the 3:2 resonance is roughly $20\text{--}100M_{\oplus}$.

The low end of this mass range is about three times the mean planet mass estimated in the preceding subsection. There are several possibilities for bridging this gap:

Test-particle calculations underestimate the dynamical effect of resonances— Our analytic calculations are only possible because one of the two planets was approximated as a test particle. If both planets have non-zero masses, the dynamical problem acquires extra degrees of freedom; even the planar single-resonance model has two degrees of freedom which allows chaos caused by overlap of the closely spaced resonances with critical angles $(p+1)\lambda_2 - p\lambda_1 - \omega_1$ and $(p+1)\lambda_2 - p\lambda_1 - \omega_2$. We have carried out exploratory integrations in which we replace the three-body system containing a planet of mass m_{pl} and a test particle with two planets of mass $m_{\text{pl}}/2$, leaving the other initial conditions and parameters the same. We find that the peaks and troughs at the 3:2 and 2:1 resonances become significantly stronger, and that a secondary peak develops narrow of the 2:1 resonance.

Long-term evolution— Systems with more than two degrees of freedom can exhibit slow evolution due to weak chaos (a classic example is the Kirkwood gaps in the asteroid belt, which can evolve on Gyr timescales; Morbidelli 1996). Integrations that follow two planets with non-zero masses, eccentricities, and inclinations may have resonant features that evolve over timescales much longer than those we have examined here.

Underestimated planet masses— Simultaneous measurements of mass and radius are available for 8 planets in the radius range $1\text{--}3R_{\oplus}$. These show an order of magnitude range of mean density, from $0.7^{+0.7}_{-0.4} \text{ g cm}^{-3}$ for Kepler 11f (Lissauer et al. 2011a) to $8.8^{+2.2}_{-2.9} \text{ g cm}^{-3}$ for Kepler 10b (Batalha et al. 2011). This wide range implies either a diverse set of planetary compositions (Wu & Lithwick

⁶ We recognize that the KS test is designed for hypothesis testing, not parameter fitting, but the data and the models do not justify a more sophisticated approach.

2012) or unmodeled errors in some or all of the measurements. In either case the actual value of the “typical” *Kepler* planet mass is far more uncertain than the simple estimate of $6\text{--}7M_{\oplus}$ obtained above. In particular, if there is a substantial population of rock-iron planets with radii of $2\text{--}3R_{\oplus}$ these would have much larger masses: for a radius of $2.3R_{\oplus}$, Seager et al. (2007) find masses of $30\text{--}200M_{\oplus}$ for a variety of rock-iron compositions, and Swift et al. (2012) find masses from $30M_{\oplus}$ for basalt to $100M_{\oplus}$ for nickel-iron planets.

7.3. Relation to previous work

Batygin & Morbidelli (2012) and Lithwick & Wu (2012) have shown that tidal dissipation can repel planet pairs from exact resonance, producing a peak wide of the resonance and a trough narrow of the resonance as observed in the *Kepler* data. However, this process requires that (i) the planet pairs form in resonance; (ii) the correct amount of dissipation is present to repel the planet pairs from resonance by a percent or so.

Moreover, if tidal dissipation from the host star were responsible for shaping the period-ratio distribution around resonances, one should expect a strong dependence on orbital radius or period (the characteristic timescale for changes in semi-major axis a varies as a^8 in the tidal evolution model of Hut 1981). However, Rein (2012) points out that the period-ratio distribution in the *Kepler* sample restricted to inner-planet periods < 5 d looks identical to the distribution restricted to inner-planet periods > 5 d. We have repeated Rein’s analysis for the restricted sample of two-planet systems used here and observe that there is a hint that the resonant features are more pronounced at the 3:2 resonance for the longer period planets, and more pronounced at the 2:1 resonance for the shorter period planets. However, the number of planet pairs in our restricted sample is too small to make a statistically significant detection of any difference.

Rein (2012) has also investigated whether stochastic migration can reproduce the *Kepler* period-ratio distribution. He argues that conventional “smooth” migration cannot reproduce the observations because it produces too many planet systems in exact resonance. However, these large pile-ups at resonance are smeared out by including stochastic forces that might be expected from the likely turbulent nature of the protoplanetary disk. He shows that for the correct combination of stochastic and smooth migration forces, the final period-ratio distribution looks similar to that of the *Kepler* planets.

We note that eccentricity measurements of near-resonant planets do not distinguish between these mechanisms: tidal dissipation damps the free eccentricity so the residual eccentricity is equal to the forced eccentricity, which is just the fixed point of the single-resonance Hamiltonian shown in Figure 2. Slow growth of the

planet causes a test particle on an initially circular orbit to follow the fixed point as the planet mass grows, so that it will also have zero free eccentricity unless it has crossed the separatrix.

8. SUMMARY

We have studied the orbital distribution of two-planet systems near first-order mean-motion resonances in the simplest possible model of planet formation: there is no energy dissipation or migration, and planets form *in situ* on circular, coplanar orbits, with masses growing at a prescribed rate. We have examined whether this toy model can explain the signatures in the period-ratio distribution near resonances that are observed in the *Kepler* sample of 242 two-planet systems.

Our approach is to construct a simplified Hamiltonian that isolates the perturbations due to a given first-order resonance. We then solve for the long-term dynamics of a test particle in this Hamiltonian, focusing on two limiting cases: rapid and slow mass growth of the planet. We have used numerical integrations of the restricted three-body problem to confirm that the resonance Hamiltonian captures the main features of the orbit evolution.

We find that the distribution in period ratios resembles a “P-Cygni” profile, where orbits are evacuated from narrow of the resonance (i.e., closer to the perturbing planet) and pile up in regions wide of the resonance. These features are present whether the planet grows fast or slowly, though they are stronger in the latter case, and hence should be present for a wide range of growth histories. The resulting structure in the period-ratio distribution is strongly reminiscent of the peak-trough feature observed at the 3:2 and 2:1 resonances in the *Kepler* systems.

The model and observed period-ratio distributions near these resonances are consistent for mean planet masses in the range $20\text{--}100M_{\oplus}$. This is larger than expected from the handful of *Kepler* planets with typical radii of $2\text{--}3R_{\oplus}$ and measured masses by a factor of 3–15. However, the mass-radius relation for *Kepler* planets is quite uncertain and shows large scatter, and the required masses are consistent with the masses expected for planets in this radius range that are composed of a mixture of silicates and iron with no extended atmosphere. Other effects such as weak chaos operating on Gyr timescales may also narrow the gap between the model and the observations. Our model suggests that the resonant features seen in the *Kepler* multi-planet systems may not require either dissipation or migration during the planet-formation process.

We are grateful to Subo Dong, Darin Ragozzine, and Hanno Rein for their insights and suggestions. RM gratefully acknowledges support from the Institute for Advanced Study, and CP acknowledges support from the CONICYT Bicentennial Becas Chile fellowship.

APPENDIX

MIGRATION SPEED AND CAPTURE INTO RESONANCE

Capture into a $(p+1) : p$ resonance during convergent migration is certain if the planets cross the resonance slowly enough and their eccentricities and inclinations are small enough. These statements can be quantified using the formalism of §2.

In convergent migration, the dimensionless resonance distance Δ (eq. 17) is increasing with time. Since the resonant

Hamiltonian K (eq. 16) is dimensionless, resonance crossing without capture should occur when $d\Delta/d\tau > g$ where g is some constant of order unity. Converting this inequality to physical units yields

$$\frac{d}{dt} \log n_{\text{pl}} > \frac{3^{5/3}g}{4} |p^2(p+1)|^{1/9} n_{\text{pl}} \left| \frac{m_{\text{pl}}}{m_*} f_p \right|^{4/3}. \quad (\text{A1})$$

Define the migration time of the massive planet to be $t_{\text{mig}} \equiv (d \log n_{\text{pl}}/dt)^{-1}$; then the condition for resonance crossing without capture is

$$t_{\text{mig}} < \frac{3.0 \times 10^4 \text{ yr}}{g w_p} \frac{P_{\text{pl}}}{100 \text{ d}} \left(\frac{10 M_{\oplus}}{m_{\text{pl}}} \frac{m_*}{M_{\odot}} \right)^{4/3} \quad (\text{A2})$$

where P_{pl} is the massive planet's orbital period and $w_p \equiv |p^2(p+1)|^{1/9} f_p^{4/3}$ is 1.363 for $p = 1$ (2 : 1 resonance) and 3.377 for $p = 2$ (3 : 2 resonance). The constant g is estimated to be 2.5 by Friedland (2001) from approximate analytic calculations and 2.7 by Quillen (2006) from numerical orbit integrations.

The maximum eccentricity at which capture into resonance is certain during convergent migration has been derived by several authors (e.g., Henrard & Lemaître 1983; Borderies & Goldreich 1984). If the eccentricity of the test particle when far from resonance is e_0 , then the area enclosed by its orbit in the x - y plane is $A_0 = \pi e_0^2/s_e^2$ (eq. 19). Because of adiabatic invariance, this area is conserved as the planet migrates. The test-particle orbit will be interior to the homoclinic orbit when it first appears, at $\Delta = 1$ (cf. Figure 1), if $A_0 < 6\pi$, the area of the homoclinic orbit. As the planet continues to migrate and Δ continues to grow, the area inside the homoclinic orbit grows so the test particle remains inside the homoclinic orbit, i.e., it remains captured in the resonance. Thus the condition that resonance capture is certain is $e_0 < \sqrt{6} s_e$ or

$$e_0 < \frac{2^{1/2} 3^{1/6}}{|p^2(p+1)|^{2/9}} \left| \frac{m_{\text{pl}}}{m_*} f_p \right|^{1/3} = 0.0528 h_p \left(\frac{m_{\text{pl}}}{10 M_{\oplus}} \frac{M_{\odot}}{m_*} \right)^{1/3}, \quad (\text{A3})$$

where $h_p = |p^2(1+p)|^{-2/9} |f_p|^{1/3}$ is 0.909 for $p = 1$ and 0.728 for $p = 2$.

REFERENCES

- Anglada-Escudé, G., López-Morales, M., & Chambers, J. E. 2010, *ApJ*, 709, 168
- Baluev, R. V. 2011, *Celestial Mechanics and Dynamical Astronomy*, 111, 235
- Batalha, N. M., Borucki, W. J., Bryson, S. T., et al. 2011, *ApJ*, 729, 27
- Batygin, K., & Morbidelli, A. 2012, arXiv:1204.2791
- Borderies, N., & Goldreich, P. 1984, *Celestial Mechanics*, 32, 127
- Delisle, J.-B., Laskar, J., Correia, A. C. M., & Boué, G. 2012, *A&A*, 546, A71
- Fabrycky, D. C., Lissauer, J. J., Ragozzine, D., et al. 2012, arXiv:1202.6328
- Friedland, L. 2001, *ApJ*, 547, L75
- Henrard, J., & Lemaître, A. 1986, *Celestial Mechanics*, 30, 197
- Hut, P. 1981, *A&A*, 99, 126
- Lecar, M., Franklin, F. A., Holman, M. J., & Murray, N. J. 2001, *ARA&A*, 39, 581
- Liou, J.C., & Malhotra, R. 1997, *Science*, 275, 375
- Lissauer, J. J., Fabrycky, D. C., Ford, E. B., et al. 2011a, *Nature*, 470, 53
- Lissauer, J. J., Ragozzine, D., Fabrycky, D. C., et al. 2011b, *ApJS*, 197, 8
- Lissauer, J. J., Marcy, G. W., Rowe, J. F., et al. 2012, *ApJ*, 750, 112
- Lithwick, Y., & Wu, Y. 2012, *ApJ*, 756, L11
- Malhotra, R. 1993, *Nature*, 365, 819
- Malhotra, R. 1994, *Physica D*, 77, 289
- Malhotra, R. 1998, in *Solar System Formation and Evolution*, eds. D. Lazzaro et al., *PASP Conference Series* 149, 37
- Malhotra, R., Black, D., Eck, A., & Jackson, A. 1992, *Nature*, 356, 583
- Minton, D. A., & Malhotra, R. 2009, *Nature*, 457, 1109
- Minton, D. A., & Malhotra, R. 2010, *Icarus*, 207, 744
- Morbidelli, A. 1996, *AJ*, 111, 2453
- Murray, C. D., & Dermott, S. F. 1999, *Solar System Dynamics* (Cambridge: Cambridge University Press).
- Murray, N., & Holman, M. 1997, *AJ*, 114, 1246
- Quillen, A. C. 2006, *MNRAS*, 365, 1367
- Rasio, F. A., Nicholson, P. D., Shapiro, S. L., & Teukolsky, S. A. 1992, *Nature*, 355, 325
- Rein, H. 2012, *MNRAS*, 427, L21
- Rein, H., Payne, M. J., Veras, D., & Ford, E. B. 2012, *MNRAS*, 426, 187
- Seager, S., Kuchner, M., Hier-Majumder, C. A., & Militzer, B., 2007, *ApJ*, 669, 1279
- Snellgrove, M. D., Papaloizou, J. C. B., & Nelson, R. P. 2001, *A&A*, 374, 1092
- Swift, D. C., Eggert, J. H., Hicks, D. G., et al. 2012, *ApJ*, 744, 59
- Tanaka, H., Takeuchi, T., & Ward, W. R. 2002, *ApJ*, 565, 1257
- Tremaine, S., & Dong, S. 2011, *AJ*, 143, 94
- Wisdom, J., 1980, *AJ*, 85, 1122
- Wisdom, J. 1983, *Icarus*, 56, 51
- Wright J. T. et al. 2011, *PASP*, 123, 412
- Wu, Y., & Lithwick, Y. 2012, arXiv:1210.7810